Available online at www.sciencedirect.com
SCIENCE DIRECT®
Physics of the Earth and Planetary Interiors 138 (2003) 55–69
PHYSICS OF THE EARTH AND PLANETARY INTERIORS
www.elsevier.com/locate/pepi

Scattering objects in the lower mantle beneath northeastern China observed with a short-period seismic array

Tadashi Kito [a,*], Takuo Shibutani [b], Kazuro Hirahara [c]

[a] *Institut für Geowissenschaften, Universität Potsdam, Postfach 601553, Potsdam D-14415, Germany*
[b] *Disaster Prevention Research Institute, Kyoto University, Kyoto, Japan*
[c] *Division of Earth and Environment Sciences, Graduate School of Environment Studies, Nagoya University, Nagoya, Japan*

Received 2 July 2002; received in revised form 5 March 2003; accepted 6 March 2003

Abstract

Precursor and coda portions of short-period PcP waves (reflected P wave from the core–mantle boundary, CMB) recorded at J-array stations in Japan were analyzed in order to extract weak scattered signals originating from small-scale heterogeneities in the lowermost mantle beneath northeastern China. Two nuclear explosions at Lop Nor in China detonated on 21 May 1992 (Mb = 6.5) and 8 June 1996 (Mb = 5.9) were used for our analysis.

Three-dimensional grids above the CMB were defined in the area around the PcP bounce points beneath northeastern China to calculate theoretical travel times of scattered waves which propagate from the sources to each grid point and arrive at each station based on the IASP91 model. Subsequently the waveforms were aligned with respect to the theoretical travel times and the semblance (an amplitude dependent measure of coherency) was calculated for each grid point. In order to obtain a more accurate travel time correction, we applied a cross correlation method to PcP waveforms in order to reduce picking error of the PcP onset time. A cross convolution method was also applied so that the two events could be analyzed simultaneously without using unstable deconvolutions.

We could identify regions with relative high semblance values in semblance contour maps at about 200 and 375 km above the CMB. Stacking waveforms with respect to the theoretical travel times for the grid points with relative high semblance values indicate coherent wavelets originating at those grid points, that is, they correspond to scattered waves originating from small-scale heterogeneities in the lowermost mantle. Our results indicate the existence of small-scale scattering objects in the D'' layer, especially in the depth range of 200 and 375 km above the CMB beneath northeastern China. Considering recent tomographic images of high velocity anomalies in this area, these scattering objects could be fragments of old oceanic crusts which have subducted through the lower mantle and have accumulated in the D'' layer beneath northeastern China.

Keywords: Seismic array; Lower mantle; Core–matle boundary

1. Introduction

The lowermost mantle, several 100 km above the core–mantle boundary (CMB), is one of the most important regions of the Earth for mantle dynamics such as mantle convection, the generation of hot plumes and the fate of subducted slabs. Heterogeneities above the CMB were first defined by Bullen (1949). It has now been recognized that the lowermost mantle, the so called D'' layer, has strong lateral variations. There are a lot of explanations for the structural heterogeneities

* Corresponding author.
E-mail address: tkito@geo.uni-potsdam.de (T. Kito).

0031-9201/03/$ – see front matter © 2003 Elsevier Science B.V. All rights reserved.
doi:10.1016/S0031-9201(03)00080-3

at the base of the mantle. A number of studies suggest that the D'' layer is a portion where subducted lithosphere may accumulate (e.g. Silver et al., 1988; Christensen, 1989; Weber, 1993; Scherbaum et al., 1997; Freybourger et al., 1999). Arrival time tomography also indicates that slabs may descend down to the CMB in some regions of the globe (Van der Hilst et al., 1997). This is not the sole explanation for the D'' layer. For instance, it has been suggested that the D'' layer is a reaction zone where lower mantle perovskite interacts with liquid iron from the outer core. Kendall and Shearer (1994) proposed a relationship between the distribution of heterogeneities and the flow in the lowermost mantle. Jeanloz and Richter (1979) and Jeanloz and Morris (1986) proposed that the D'' layer is a thermal boundary layer which is formed by heat flow from the outer core.

The first discovery of triplication of S waves in the distance range from 70 to 95° by Lay and Helmberger (1983) suggests that the top of the D'' layer is a first-order discontinuity with 2–3 % velocity jump at a depth of about 2620 km beneath the central America. This study indicates that the D'' layer may be a material boundary layer whose depth can vary by about 40 km. Regarding P waves, a first-order discontinuity at the top of the D'' layer was first proposed by Wright et al. (1985).

The existence of precursors to core phases of PKP and PKKP, travel time anomalies of short-period PcP and PKIKP or long-period P-diffracted waves and the discovery of triplication of S wave has led to a general model of heterogeneities near the CMB. As seismological observations have accumulated, it has been recognized that the lowermost mantle has even more heterogeneities than previously considered. Using tomographic methods, Fukao (1993) found a 1% anomaly in P wave velocity on a global scale at the depth range of 2700–2900 km. This 1% perturbation is too large for the D'' layer to be a thermal discontinuity. They suggest that high velocity anomalies in the D'' layer can be related to subducted old oceanic plates, which were first deposited on the bottom of the upper mantle (at the 660 km discontinuity) and finally dropped into the D'' layer, because the distribution of high velocity anomalous regions in the mantle transition zone is relatively similar to that of high velocity anomalous regions in the lowermost mantle.

Haddon and Cleary (1974) found precursors of PKP waves and suggested that one possible structure which could produce such precursors is a 200 km thick in the radial direction and 30 km long in the lateral direction D'' layer with velocity perturbations of the order of 1%. But such precursors can also be explained by a 300 m amplitude undulation of the CMB (Bataille et al., 1990). Studies of the structure near the CMB using travel time anomalies estimate large-scale heterogeneity with a scale length of more than 100 km. On the other hand, Cleary and Haddon (1972) interpreted the observed short-period precursors to PKIKP as waves scattered from small-scale heterogeneities existing near the CMB. Since their work, the detailed structure of small-scale heterogeneities has been revealed by the precise determination of scattered core waves: short-period wave trains which are precursors to PKIKP, PKKP, and PKPPKP. The analysis of these scattered waves has been based on the single scattering theory using Born approximations (e.g. Doornbos, 1978; Aki, and Richards, 1980). The heterogeneities have been quantitatively estimated by using either global network data (e.g. World Wide Standardized Seismic Network (WWSSN) and Global Digital Seismic Network (GDSN) or array observation (e.g. NORSAR). But it is still difficult to determine which is the cause of the primary scattering structure: volumetric heterogeneities near the CMB or undulation of the CMB topography.

Furumoto (1992) estimated the topography of the CMB using steep angle scattered waves, which do not propagate along the great circle path. These migration methods could be powerful tools for detecting the small scale of heterogeneities near the CMB. Another seismic wave which can be used to detect the structure of the CMB and the D'' layer is the PdP phase, a reflected wave from the top of the D'' layer (Weber and Davis, 1990; Weber, 1993). Although PdP phases can be a powerful tool to detect a discontinuity in the D'' layer, the detectable area is fairly limited, because the reflected points of PdP are restricted to the great circle path and large reflection coefficients of PdP are restricted to the epicentral distances between 50 and 70°.

In this study, we investigate the steep angle scattering of P wave in the lowermost mantle with the prominent period of 1 Hz. The scattering P waves used in this study are no reflected waves. Therefore, they

do not obey Snell's law at the scattering points in the sense that incident angle and reflected angle are not same. Most scattering waves do not propagate along the great circle path. Our epicentral distance ranges from 33 to 42° and the study area is located beneath the east side of the Gobi desert. The lowermost mantle in this region belongs to a high P wave velocity anomalous zone in the tomographic study by Fukao (1993) and Boschi and Dziewonski (1999).

2. Data

We used short-period seismic data from nuclear explosions at Lop Nor in China detonated on 21 May in 1992 (Event_92) and on 8 June in 1996 (Event_96) recorded at J-array stations (Shibutani et al., 1999) and at the short-period seismological networks of the Research Center for Earthquake Prediction of Hokkaido University, the Earthquake Research Institute, University of Tokyo and the Research Center for Earthquake Prediction, Disaster Prevention Research Institute, Kyoto University, respectively. The J-array is a large-aperture short-period seismic array, which stretches 3000 km along the Japan Islands and is 500 km wide. It consists of more than 200 stations with vertical components, most of which have seismometers with a natural frequency of 1 Hz (J-array Group, 1993). We used the data from the J-array for Event_92 and collected the data from the short-period seismological networks of the above three institutes for Event_96. The sampling rate varies between data,

Table 1
Source parameters for Event_92 and Event_96

Event	Date	Time	Longitude	Latitude	Mb	No. of traces
Event_92	21 May 1992	04:59:57.7	88.813	41.604	6.5	76
Event_96	8 June 1996	02:55:58.0	88.690	41.657	5.9	72

Origin time, longitude, latitude, body wave magnitude and the number of waveforms used in this study. The parameters are taken from Preliminary Determination of Epicenters (PDE).

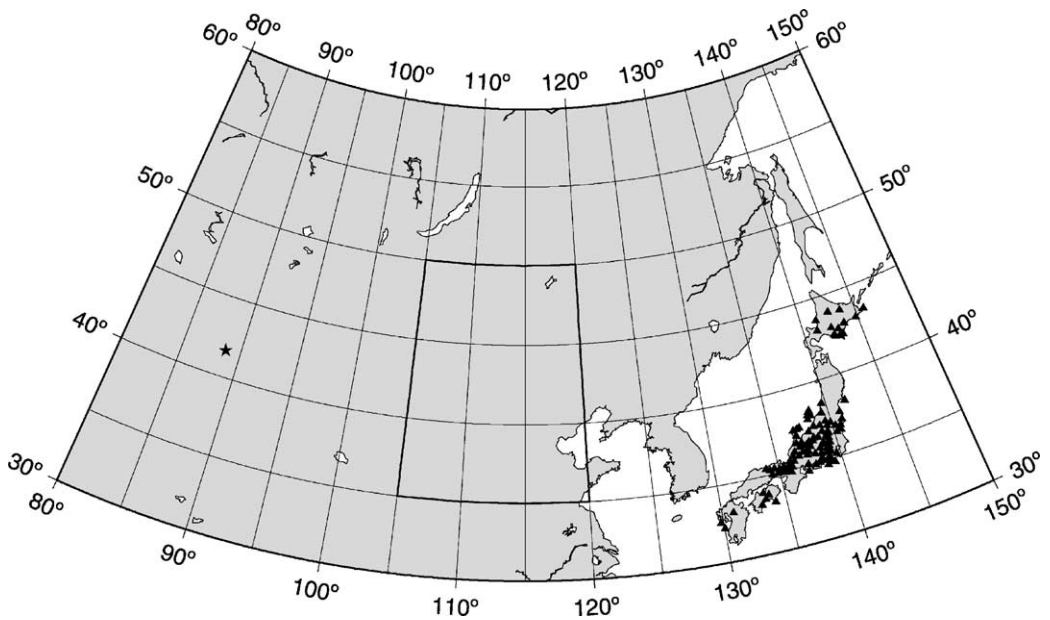

Fig. 1. Map showing locations of epicenter of events (star) and distribution of stations (triangle). Our target is the lowermost mantle beneath the area enclosed by a bold line.

so we resampled these data to a sampling rate of 20 Hz. Origin times and source parameters were taken from Preliminary Determination of Epicenters (PDE). The parameters are shown in Table 1. We selected traces with good signal to noise ratios for each event to get clear PcP waves, since the waveforms of PcP should be similar among the events in the stacking process. The number of selected stations of Event_92 and Event_96 are 76 and 72, respectively. The station–source geometry is shown in Fig. 1.

3. Data preprocessing (cross convolution method)

A band pass filter with corner frequencies of 0.5 and 2.0 Hz was applied to the raw data in order to remove unexpected signals that were more influenced by local structures just beneath the stations. Since the individual seismometer magnifications of the J-array stations are not well known, we normalized each trace by the maximum amplitude of PcP. Though an advantage of using nuclear explosions is that their source time functions are quite simple in comparison with those of natural earthquakes, the pulse widths of PcP-beams of two events are quite different due to differences of the source time functions (Fig. 2). In order to correct the pulse widths and waveforms, we used a cross convolution method in which we convolved the source time function of one event with the traces of the other event. In other words, the PcP-beam of Event_92 was convolved with each trace from Event_96 and the PcP-beam of Event_96 was also convolved with each trace from Event_92 in the same way. A benefit of our method is that we can avoid instability of deconvolution which can distort waveforms when the vales of the denominator spectrum are very small. After applying the cross convolution method, we find quite similar PcP waveforms throughout the data. The cross convolved data sets with static station correction described in the next section are shown in Fig. 3(a) for Event_92 and in Fig. 3(b) for Event_96.

4. Static station correction

Since the Pacific plate and the Philippines sea plate are subducting under the Japan Islands from the east and the south, respectively, strong heterogeneities just beneath the Japan Islands influence the incoming P and PcP wave fields. One possible reason for the time delay of P and PcP with respect to IASP91 is the mantle wedge beneath the Japan Islands where seismic waves propagate slower than the other areas. Since the J-array stations extend over the whole Japan Islands,

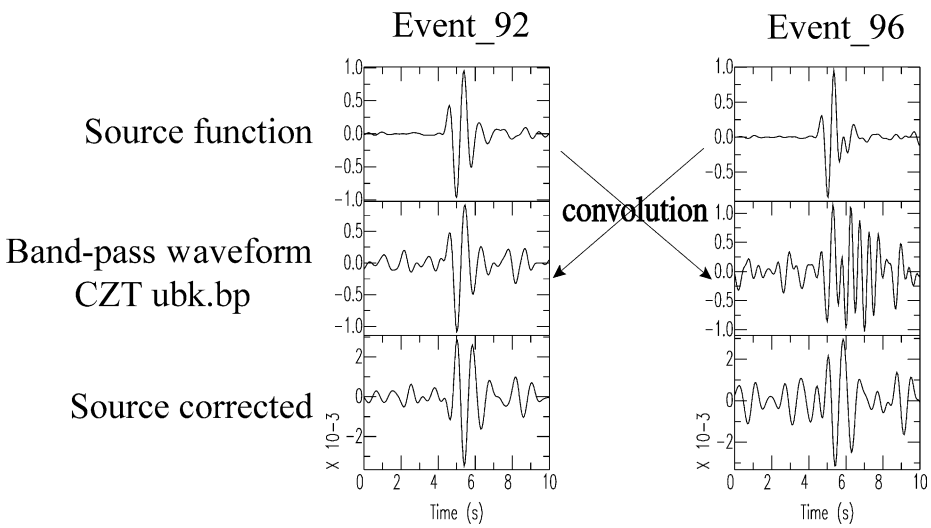

Fig. 2. Example of source time function equalization using the cross convolution method. The upper waveforms show the source time function obtained by stacking PcP for each event. The middle waveforms are examples of observed data for PcP (here CZT). The lower waveforms show the resulting waveform after the cross convolution.

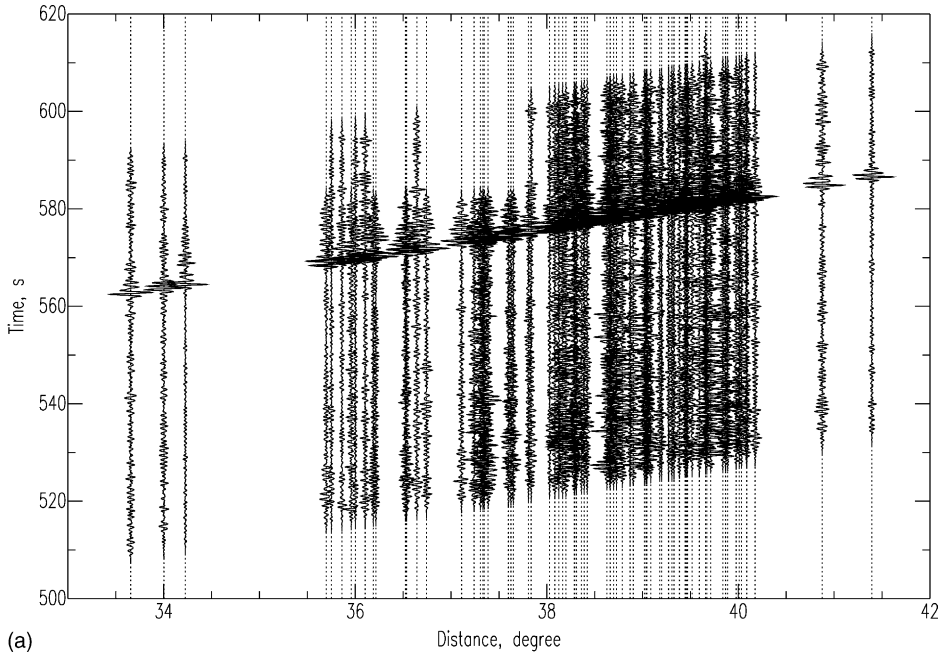

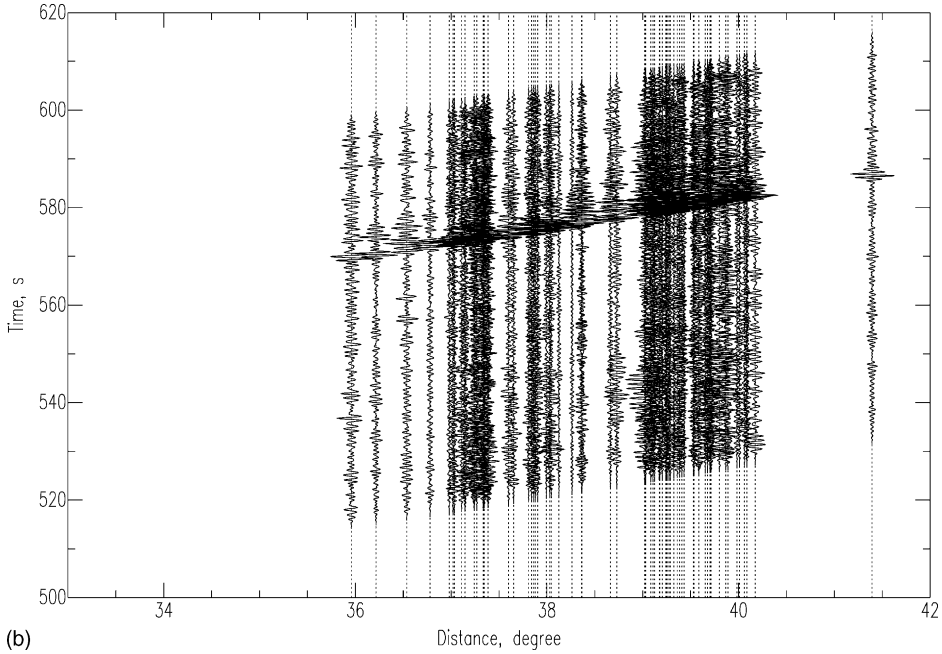

Fig. 3. (a and b) Waveform data sets used for our analysis sorted by epicentral distance. The dominant signals in the middle are PcP: (a) Event_92 and (b) Event_96.

local structures near in the stations are different from each other, which causes travel time anomalies of P and PcP waves. In order to remove the effect of the heterogeneities in the upper mantle and in the crust and the elevation of stations, the PcP waves of each trace are aligned with respect to the IASP91 model (Kennett and Engdahl, 1991). These travel time corrections of PcP waves can be considered as station corrections for the scattered waves originating from the lowermost mantle, because the paths of PcP wave and the scattered waves for one station are quite similar in the upper mantle and the crust. We assumed that the PcP waves propagate along the great circle path between sources and stations. A travel time correction of the i-th station can be expressed by the following equation.

$$\Delta t_i = \mathrm{PcP}_i^{\mathrm{obs}} + C_i - \mathrm{PcP}_i^{\mathrm{iasp91}}, \quad (1)$$

where $\mathrm{PcP}_i^{\mathrm{obs}}$ is the observed travel times of PcP of i-th station and $\mathrm{PcP}_i^{\mathrm{iasp91}}$ is the theoretical travel time of PcP based on the IASP91 earth model (Kennett and Engdahl, 1991). C_i is a correction for the picking error of the PcP onset time, which could be obtained by the following procedures. First, the PcP waves were aligned with respect to the theoretical travel time and were stacked in order to obtain a PcP-beam. Subsequently, cross correlations between each PcP waveform and the PcP-beam were taken to estimate the differences of the waveforms. When the correlation was maximized, the time difference C_i was calculated. This procedure would continue until the time difference C_i became invariant. Using four iterations of this method, we could increase the sum of the square of the PcP-beam in the time window from 0.3 s before the PcP onset time to 1.7 s after the PcP onset time by 10.6%. The resulting seismograms are shown in Fig. 3(a) and (b) for each event. We can recognize that the PcP waveforms equalized. The resulting static station corrections are positive values at all stations with a mean value of 1.20 s and a standard deviation of 0.48 s.

5. Method

In order to extract small amplitude scattered waves, a migration method was used in this study. First, we defined three-dimensional grids from the CMB (2889 km) up to 500 km above the CMB with vertical and lateral spacing 25 km and 0.5°, respectively. (See the box in Fig. 1 for the lateral dimensions of the grid volume). We calculated the theoretical travel time of scattered waves which propagate from the sources to a specific grid point, are scattered there and finally arrive at the stations. This calculation was carried out based on the IASP91 earth model (Kennett and Engdahl, 1991). Based on the theoretical travel time, we estimated amplitude dependent coherency of waves scattered in the lower mantle by semblance analysis, assuming isotropic single point forward scattering. The method we used is closely related to the "source array method" developed by Krüger et al. (1993, 1995, 1996), Scherbaum et al. (1997), Kaneshima and Helffrich (1998), and Thomas et al. (1999). We assume that converted waves and scattered waves which are generated by the heterogeneities near the stations have almost no influence on our semblance analysis because these waves are offset by the stacking process and the amplitude of these waves become very small.

6. Semblance

Semblance is defined by the following equation:

$$S = \frac{\sum_{j=1}^{K}\left[\sum_{i=1}^{M} f_i\left(t_j - \mathrm{SCAT}_i^{\mathrm{iasp}} - \Delta t_i\right)\right]^2}{M\sum_{j=1}^{K}\sum_{i=1}^{M} f_i\left(t_j - \mathrm{SCAT}_i^{\mathrm{iasp}} - \Delta t_i\right)^2}, \quad (2)$$

where K defines the time window, M is the number of stations used for the analysis, f_i the waveform at the i-th station, and the t_j is j-th sampling. Δt_i is the static station correction which is defined by the Eq. (1) and $\mathrm{SCAT}_i^{\mathrm{iasp}}$ is the theoretical travel time of the scattered waves based on the IASP91 earth model. The time window is the duration of the stacked PcP.

The semblance value indicates an amplitude dependent measure of the coherency of scattered waves and can take values between 0 and 1, though the semblance itself is unitless. A semblance value of 1 means that the waveforms are perfectly coherent and the amplitude of the waveforms are same, and a semblance value of 0 means that the waveforms are totally incoherent, both of which are rarely observed in the waveform data. A semblance value for same waveforms whose

amplitudes are different is, however, not equal to 1, namely, the amplitude differences among the traces can affect semblance values. It is noted that the semblance includes not only coherency information, but also information of amplitude differences among the traces.

7. Results

Fig. 4 shows the distribution of semblance values on the CMB. Around a point (42°N, 114°E) where there are numerous PcP reflection points, many grid points show quite high semblance values. The maximum value of the semblance is 0.423. The semblance values are not 1 in the area of the PcP bounce points because it has never happened that PcP waves were aligned with respect to the theoretical travel time of PcP on any grid point in the migration method.

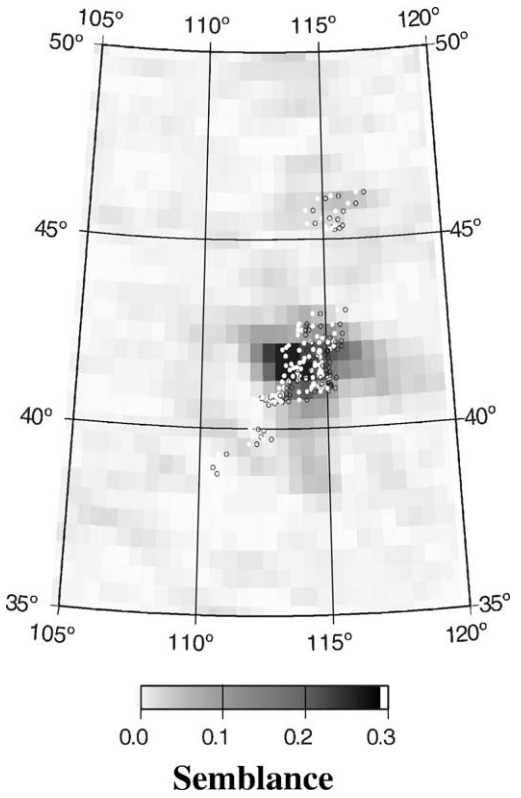

Fig. 4. Lateral distribution of semblance value at the CMB. Open symbols indicate theoretical PcP bounce points for each station.

Semblance values around the PcP reflection points corresponding to Kyushu, Shikoku and Hokkaido are quite low because of the small number of stations. The distributions of the semblance for each grid and depth (vertical interval 25 km) are shown in Fig. 5. Depth is indicated by distance from the CMB. Some regions with relative high semblance values are visible between 25 and 125 km above the CMB. The relative high semblance values in these regions indicate PcP energy. Since PcP waves have very large amplitude in comparison with the scattered waves from the heterogeneities in the lower mantle, the PcP waves themselves can disturb the estimation of the scattered waves. At depths of about 200 and about 375 km above the CMB, we can see some relative high semblance values which are not contaminated by PcP phases. Histograms of all grid points in the depth range from 150 to 500 km above the CMB are shown in Fig. 6; in this depth range, PcP energy does not have an effect on the semblance values. The histogram indicates that 5% of the grid points have semblance values higher than 0.015 and 10% of the grid points show semblance values higher than 0.011. Some stacked waveforms corresponding to the theoretical travel time for grid points with relative high semblance values are shown in Fig. 7. Relative large amplitude wavelets with several peaks are clearly visible just after the theoretical travel times in each stacked waveform. The top waveform is a stacked wave with respect to one grid point on the CMB, where large PcP energy is coming. The other waveforms are stacked waves from the grid points in the D'' layer which have relative high semblance values. These waveforms are quite similar to that of PcP. The peak semblance value of 0.03, obtained from the histogram (Fig. 6) can be considered as a semblance value generated by just random noise. On the other hand, the grids whose semblance value are larger than 0.015 are just 5% of the grid points in the depth range from 150 to 500 km above the CMB. Since the amplitude of stacked waveforms for the grid points with relatively large semblance values are significantly larger than those of noise portion of the waveforms, it is likely that lower mantle scattered waves are observed from grid points with semblance value larger than 0.015. Therefore, we conclude that these grid points act as a scattering volume, although the lower limit of the semblance value indicating truly scattered waves is imprecisely defined. The

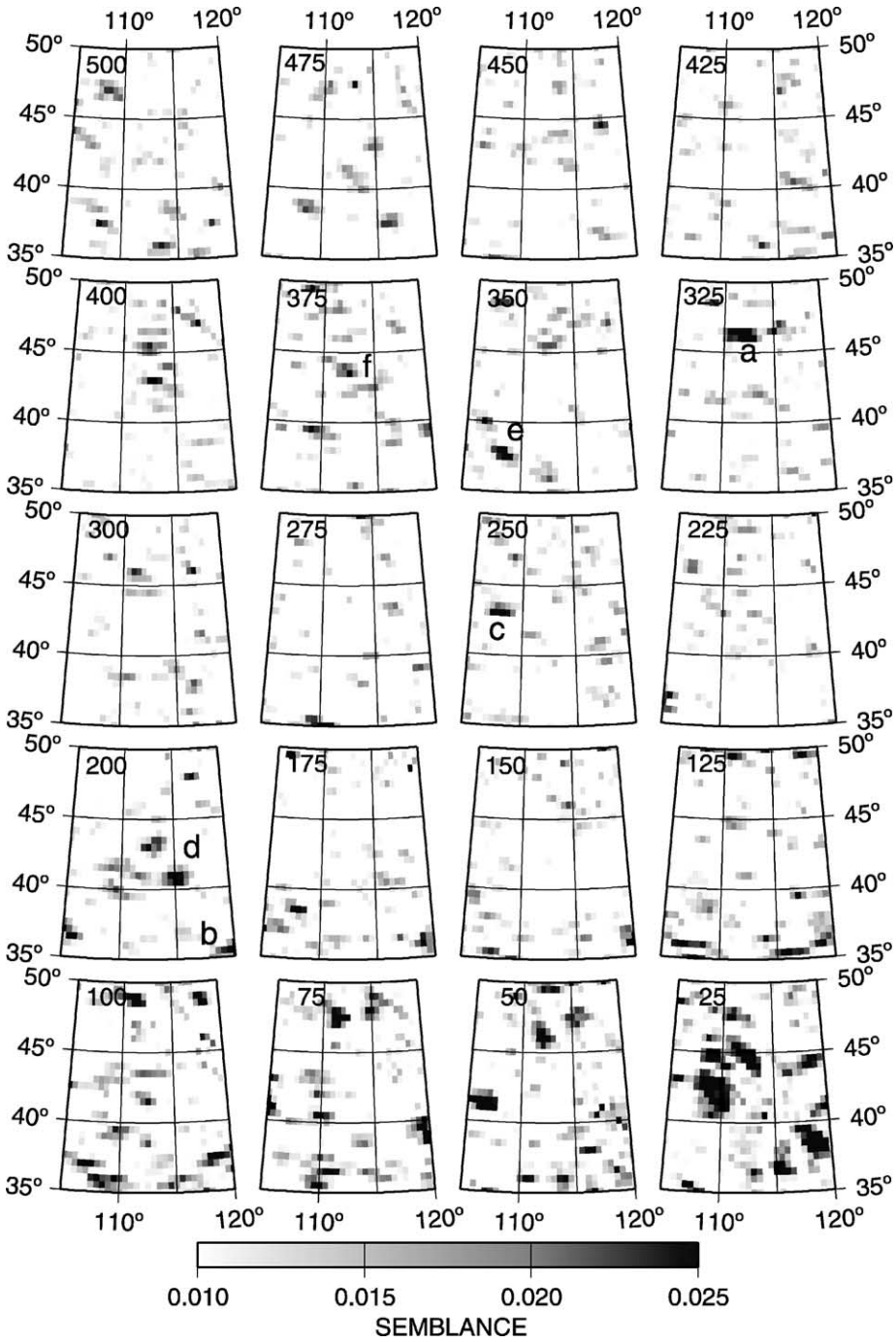

Fig. 5. Distribution of semblance value between 25 and 500 km above the CMB. The numbers at the upper left of each figure indicate distance from the CMB. Vertical and horizontal axes are latitude and longitude, respectively. The lower limit in the scale is 0.011. High semblance values effected by PcP energy reach the highest limit.

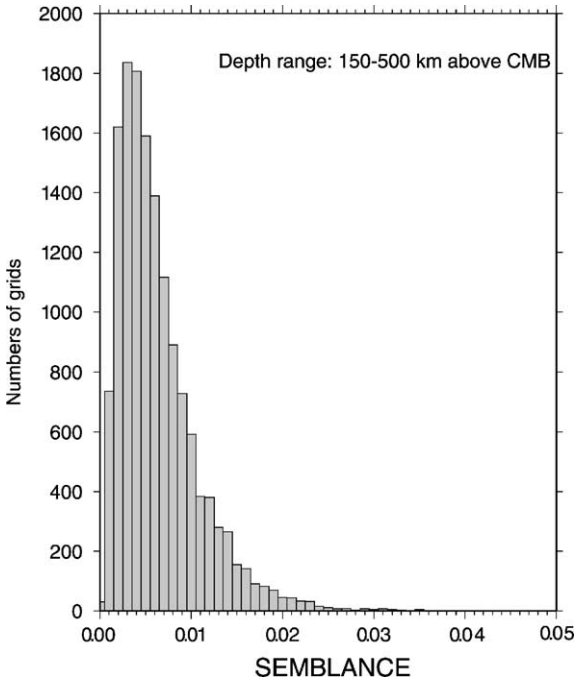

Fig. 6. Histogram of the semblance distribution for all grid points in the depth range between 150 and 500 km above the CMB.

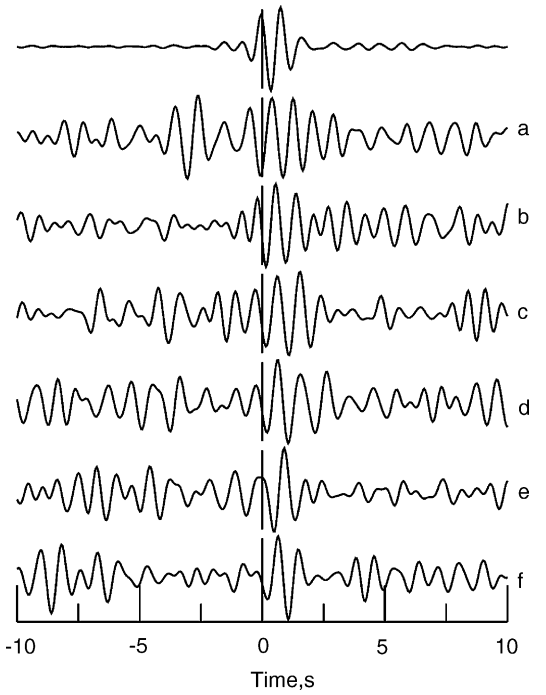

Fig. 7. Examples of waveforms stacked with respect to the theoretical travel times of grid points whose semblance values are relatively high (labeled a–f in Fig. 5). Lines in the each indicate the theoretical travel time for each grid. The uppermost trace is waveform stacked with respect to one grid point on the CMB, where PcP energy is coming. In other traces relative large amplitude wavelets are seen just after the theoretical travel time.

distribution of semblance values larger than 0.015 is shown sorted by depth in Fig. 8. Since the grid points within 125 km above the CMB are contaminated by the PcP phases, these grid points are removed from the discussion. In the depth range between 150 and 500 km above the CMB, there are two remarkable peaks at about 200 and about 375 km above the CMB, respectively. In the depth range between 275 and 300 km above the CMB and around 450 km above the CMB, few scattering volumes are observed. The same patterns for the distribution of scattering volumes can also be recognized in Fig. 5. Another noticeable feature is that frequency of the scattering volume is decreasing from 200 to 150 km above the CMB.

8. Estimation of the semblance values

A bootstrap analysis was carried out in order to estimate confidence of the semblance values. First, 148 traces (same number of traces used in the semblance analysis) were randomly selected from the original station group, allowing overlapping. This group of selected stations is called the bootstrap sample. In this study, there are 100 bootstrap samples. For these bootstrap samples, semblance values were calculated for each grid point in the same way as described in the chapter 5. Fig. 9 shows the mean values of the resulting semblance values obtained from all bootstrap samples for each grid point. These mean semblance values should be more stable than the semblance values shown in Fig. 5, because mean values of the relative high semblance are unlikely to be produced by noise by chance in the bootstrap analysis. The areas marked by a–f in Fig. 5, where the relative high semblance values were observed, can more or less be recognizable in Fig. 9, though some areas are not clearly identified.

The same bootstrap analysis was carried out using synthetic random noise (white noise) data in order to estimate a noise level. Random noise is considered as

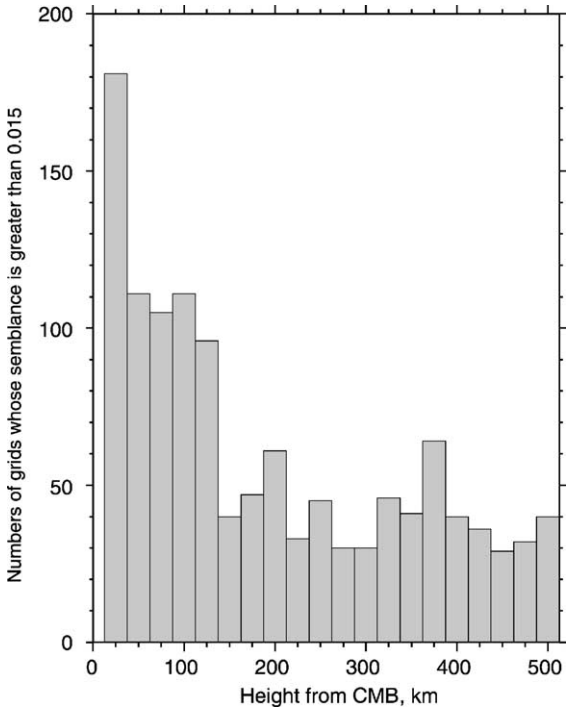

Fig. 8. Depth distribution of the numbers of grid points whose semblance value is larger than 0.015.

totally incoherent wavelets without a significant signal. Since white noise can contain every frequency wavelet, the noise data were filtered with corner frequencies of 0.5–2.0 Hz. The number of traces in the noise data is same as that in the observed one (148). The mean semblance values were calculated in the same way. In Fig. 10, mean values of the semblances obtained from bootstrap samples by using white noise data set are shown. A comparison between observed data and synthetic noise data clearly shows that the former contains significantly high semblance values.

Fig. 11 shows histograms of the mean semblance values in the bootstrap samples for the observed data and the noise data. In comparison with the result of the semblance analysis, the semblance values obtained by the bootstrap method are slightly higher on the whole. This is probably due to repetition of the same stations in the bootstrap sample. The maximum semblance value in the noise data is 0.033. This maximum value can be considered as an upper limit for the noise data. As semblance values greater than 0.033 exist in the observed data, there must be some coherent signals from the lowermost mantle. This upper limit of 0.033 can shift, when the semblance values are calculated in the 'normal' (without bootstrap method) way. Here, we can say that all area where semblance values are greater than 0.033 would be anomalous region.

9. Discussion and interpretation

Castle et al. (2000) produced a shear wave velocity map at the base of the mantle using ScS-S and Sdiff-SKS residual travel times. They suggest that the fast velocities in their model correlate well with old subduction zones, implying that slabs reach the bottom of the mantle in 90 million years and reside there for at least another 90 million years. Since our study area is a typical high velocity anomalous region, it is very reasonable to propose that our scattering objects are fragments of old oceanic materials which have subducted from the Pacific Ocean.

There are some S wave velocity models which have strong negative velocity gradient in the lowermost mantle (Young and Lay, 1987; Garnero et al., 1988; Lay and Young, 1989; Gaherty and Lay, 1992; Garnero et al., 1993a,b; Vinnik et al., 1989). P wave velocity models with 5% low velocity zone in the lowermost mantle have been also suggested (Garnero et al., 1993a,b). These studies strongly suggest that partial melting in the lower part of D'' layer is generated due to heat from the outer core. If these results are taken into consideration, one possible reason for relative few scattering volumes in the depth range from 200 to 150 km above the CMB is that the old subducted oceanic materials are homogenized by the heat from the outer core. Our result that the scattering volume decreases from 200 to 150 km above the CMB is consistent with this assumption. However, we cannot confirm this hypothesis, because we could not investigate the structure in the depth range from the CMB to 125 km above the CMB due to the contamination from PcP waves.

The size of the effective Fresnel zone on the CMB for P waves at 1 Hz and the epicentral distances considered here are about 1°N–S and about 2°E–W. In the case of strong velocity anomalies which are significantly smaller than the Fresnel zones, the scattered wave will be smoothed in the observed wave field at

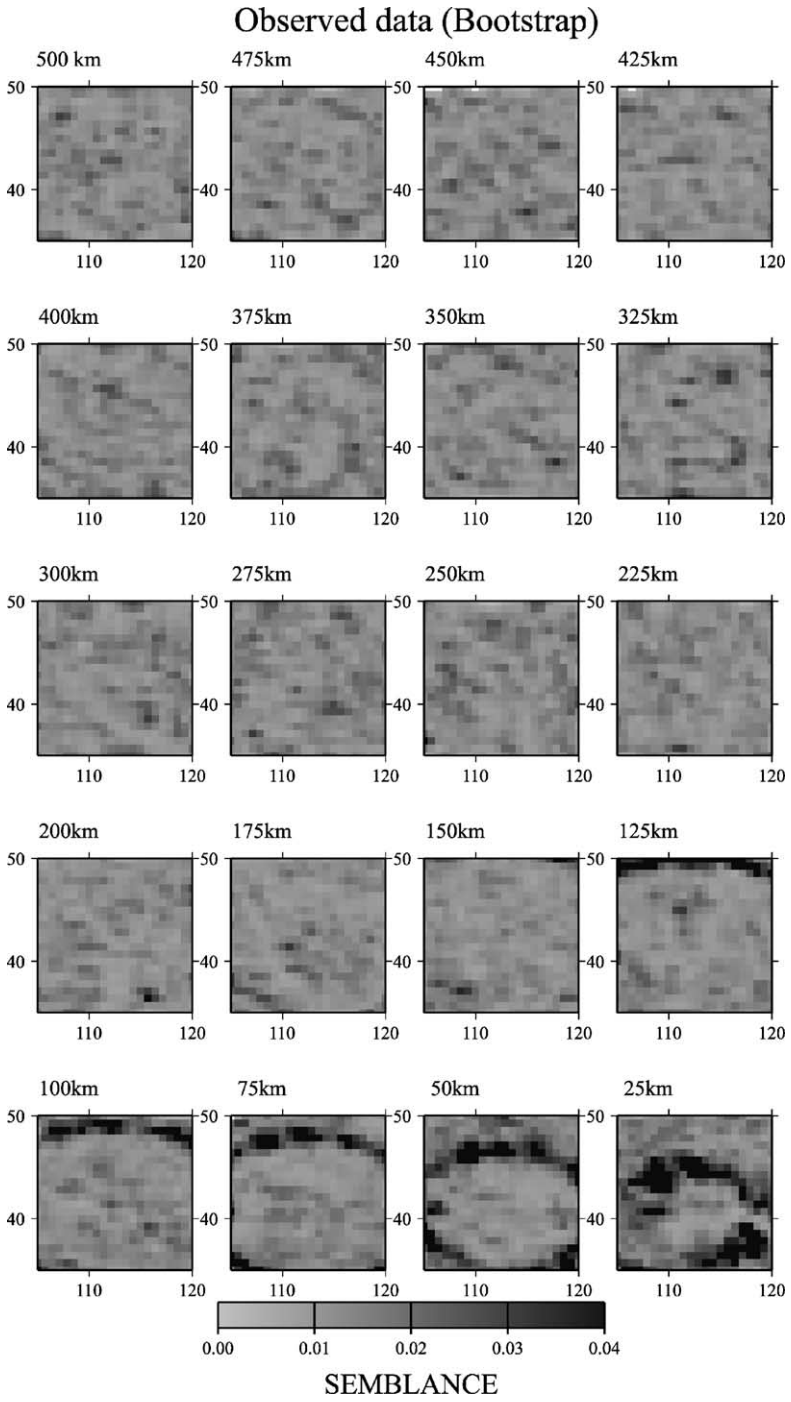

Fig. 9. Distribution of semblance value between 25 and 500 km above the CMB obtained by the bootstrap method using observed data.

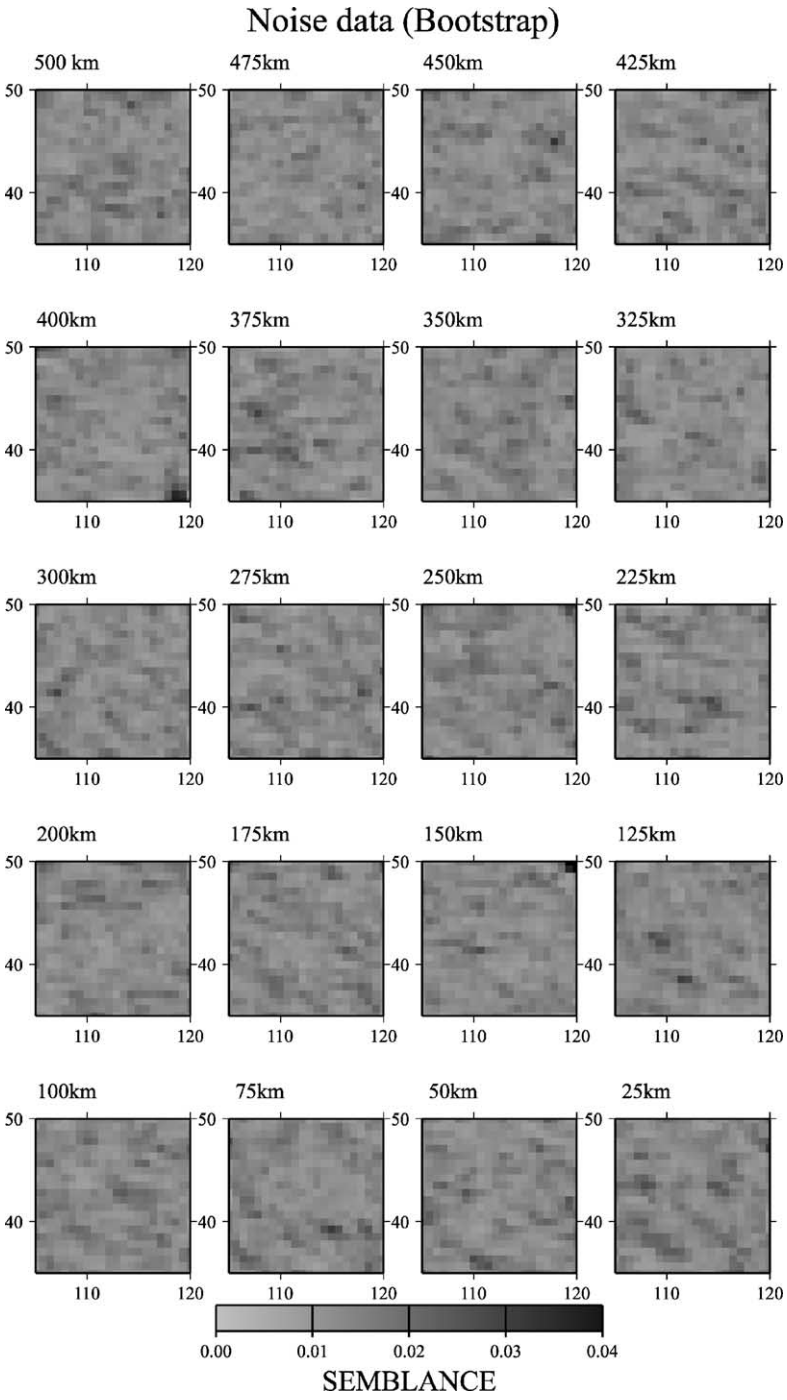

Fig. 10. Distribution of semblance value between 25 and 500 km above the CMB obtained by the bootstrap method using noise data.

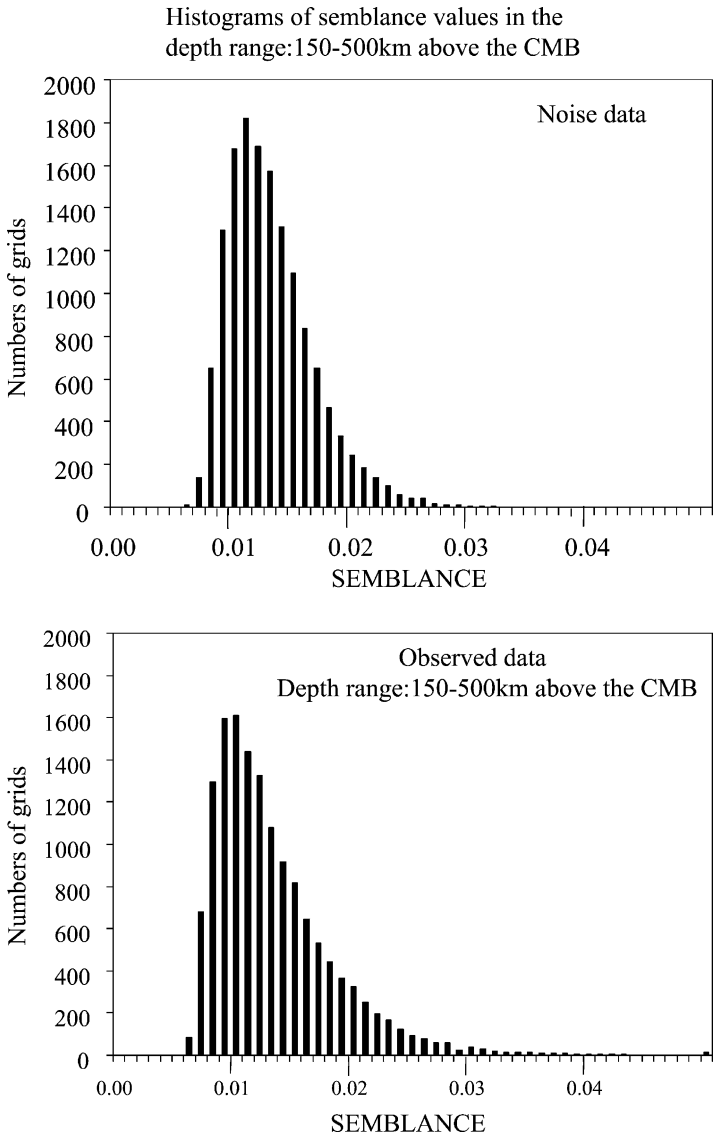

Fig. 11. Histograms of the mean semblance values distribution for all grid points in the depth range between 150 and 500 km above the CMB with noise data and (upper panel) and observed data (lower panel) calculated by the bootstrap method.

the surface by wave front healing effects (Emmerich, 1993), which is making the actual size of such small structures difficult to resolve.

Weber and Körnig (1992) suggest small-scale variations of the D'' layer in various regions all over the world and Vidale and Benz (1993) reported a secondary arrival to P wave in the epicentral distances range between 92 and 103° using the Chinese nuclear explosion which is used in this study. Although the fine structure of the D'' layer is difficult to determine, we think that the D'' layer we are detecting here using scattered waves may have a kind of different nature, that is, the shape of the D'' layer beneath the northeastern China is less likely flat, while the shape of the

D'' layer which can generate reflected waves observable in a broad distance range (more than 60°) is more or less flat. Our result indicates that heterogeneities which may not be detected by PdP exist in the D'' layer.

Yamada and Nakanishi (1993) suggest that there is no significant discontinuity which can generate reflected waves such as PdP in the lowermost mantle beneath the eastern China region (our study area). Their results indicated that the P wave impedance contrast across the upper boundary of the D'' layer in this region could be less than 2%. Since the reflection coefficient of PdP in the epicentral distance range of 40° is rather small and the heterogeneities we are detecting here using scattered waves do not necessarily generate reflected waves, our results are not necessarily inconsistent with their results.

Scherbaum et al. (1997) reported scattering volumes within the lower mantle below the Arctic in the depth range between the CMB up to 500 km. They suggested a connection between these anomalies and the Mesozoic to Cenozoic subduction of the Pacific and Kula plates. Freybourger et al. (2001) found finite size scattering objects characterized by an anisotropic scattering diagram beneath northern Siberia, which may be related to the existence of ancient subducted plate in the D'' layer. The joint interpretations of our results with those of the previous studies imply that fragments of the old oceanic crusts can be observable in the migration methods and are the first possible reason for producing the anomalous phases from the lowermost mantle.

10. Conclusions

Scattering objects in the lowermost mantle beneath northeastern China can be detected using data from 1992 and 1996 Chinese nuclear tests recorded by the J-array and by the short-period seismological networks in Japan. At depths of about 200 and 375 km above the CMB there are dominant peaks in the depth distribution of scattering objects. We think that these scattering objects represent fragments of old oceanic crusts which have accumulated over several million years in the D'' layer. Determining the fine structure, geometry and nature of the scattering volume will necessitate further array studies with better azimuthal coverage.

Acknowledgements

This study is supported by research expenses from Building Research Institute, Ministry of Land, Infrastructure and Transport. We are grateful to members of the J-array project for use of the data. We thank Institute of Seismology and Volcanology, Hokkaido University, Earthquake Research Institute, University of Tokyo and Disaster Prevention Research Institute, Kyoto University for providing us with their valuable data. We are also indebted to F. Krüger and F. Scherbaum (Institute of Geosciences, University of Potsdam) for fruitful discussions and suggestions.

References

Bataille, K., Wu, R.S., Flatte, S.M., 1990. Inhomogeneities near the core–mantle boundary evidenced from scattered waves: a review. Pure Appl. Geophys. 132, 151–173.

Boschi, L., Dziewonski, A.M., 1999. High- and low-resolution images of the Earth's mantel: implications of different approaches to tomographic modeling. J. Geophys. Res. 104, 25567–25594.

Bullen, K.E., 1949. Compressibility–pressure hypothesis and Earth's interior. Mon. Not. R. Astron. Soc., Geophys. Suppl. 5, 355–368.

Castle, J.C., Creager, K.C., Winchester, J.P., van der Hilst, R.D., 2000. Shear wave speeds at the base of the mantle. J. Geophys. Res. 105, 21543–21557.

Christensen, U.R., 1989. Models of mantle convection: one or several layers. Phil. Trans. R. Soc. Lond., Ser. A 328, 417–424.

Cleary, J.R., Haddon, R.A.W., 1972. Seismic wave scattering near the CMB: a new interpretation of precursors to PKP. Nature 240, 549–551.

Doornbos, D.J., 1978. On seismic-wave scattering by a rough core–mantle boundary. Geophys. J. Roy. Astron. Soc. 53, 643–662.

Emmerich, H., 1993. Theoretical study on the influence of CMB topography on the core reflection ScS. Phys. Earth Planet. Int. 80, 125–134.

Freybourger, M., Krüger, F., Achauer, U., 1999. A 22° long seismic profile for the study of the top of D''. Geophys. Res. Lett. 26, 3409–3412.

Freybourger, M., Chevrot, S., Krüger, F., Achauer, U., 2001. A waveform migration for the investigation of P wave structure at the top of D'' beneath northern Siberia. J. Geophys. Res. 106, 4129–4140.

Fukao, Y., 1993. Seismic tomogram of the earth's mantle: geodynamic implications. Science 258, 625–630.

Furumoto, M., 1992. Fine topography of the core–mantle boundary inferred from scattered S waves. Central Core Earth 2, 345–348.

Gaherty, J.B., Lay, T., 1992. Investigation of laterally heterogeneous shear velocity structure in D'' beneath Eurasia. J. Geophys. Res. 97, 417–435.

Garnero, E., Helmberger, D.V., Engen, G., 1988. Lateral variations near the core–mantle boundary. Geophys. Res. Lett. 15, 609–612.

Garnero, E., Grand, S.P., Helmberger, D.V., 1993a. Low P wave velocity at the base of the mantle. Geophys. Res. Lett. 20, 1843–1846.

Garnero, E., Helmberger, D.V., Grand, S., 1993b. Preliminary evidence for a lower mantle shear wave velocity discontinuity beneath the central Pacific. Phys. Earth Planet. Int. 79, 335–347.

Haddon, R.A., Cleary, J.R., 1974. Evidence for scattering of seismic PKP waves near the core–mantle boundary. Phys. Earth Planet. Int. 8, 211–234.

J-array Group, 1993. The J-Array Program: System and present status. J. Geomag. Geolectr. 45, 1265–1274.

Jeanloz, R., Morris, S., 1986. Temperature distribution in the crust and mantle. Ann. Rev. Earth Planet. Sci. 14, 377.

Jeanloz, R., Richter, F.M., 1979. Convection, composition, and thermal state of the lower mantle. J. Geophys. Res. 84, 5497–5504.

Kaneshima, S., Helffrich, G., 1998. Detection of the lower mantle scatterers northeast of the Mariana subduction zone using short-period array data. J. Geophys. Res. 103, 4825–4838.

Kendall, J.M., Shearer, P.M., 1994. Lateral variations in D'' thickness from long-period shear wave data. J. Geophys. Res. 99, 11575–11590.

Kennett, B.L.N., Engdahl, E.R., 1991. Traveltimes for global earthquake location and phase identification. Geophys. J. Int. 105, 429–465.

Krüger, F., Weber, M., Scherbaum, F., Schlittenhardt, J., 1993. Double beam analysis of anomalies in the core–mantle boundary region. Geophys. Res. Lett. 20, 1475–1478.

Krüger, F., Weber, M., Scherbaum, F., Schlittenhardt, J., 1995. Evidence for normal and inhomogeneous lowermost mantle and core–mantle boundary structure under the Arctic and northern Canada. Geophys. J. Int. 122, 637–657.

Krüger, F., Scherbaum, F., Weber, M., Schlittenhardt, J., 1996. Analysis of asymmetric multipathing with a generalization of the double-beam method. Bull. Seismol. Soc. Am. 86, 737–749.

Lay, T., Helmberger, D.V., 1983. A lower mantle S wave triplication and the shear velocity structure of D''. J. Geophys. Res. 75, 799–838.

Lay, T., Young, C.J., 1989. Waveform complexity in teleseismic broadband SH displacements: slab diffractions or deep mantle reflections ? Geophys. Res. Lett. 16, 605–608.

Scherbaum, F., Krüger, F., Weber, M., 1997. Double beam imaging: mapping lower mantle heterogeneities using combinations of source and receiver arrays. J. Geophys. Res. 102, 507–522.

Shibutani, T., Ando M., Hirahara, K., 1999. J-Array Project Seismic Data Now on CD-ROM, EOS. Transactions, American Geophysical Union, vol. 80, p. 68.

Silver, P.G., Carlson, R., Olson, P., 1988. Deep slabs, geochemical heterogeneity and the large-scale structure of mantle convection: investigation of an enduring paradox. Ann. Rev. Earth Planet. Sci. 16, 477–541.

Thomas, C., Weber, M., Wicks, C.W., Scherbaum, F., 1999. Small scatterers in the lower mantle observed at German broadband arrays. J. Geophys. Res. 104, 15073–15088.

Van der Hilst, R.D., Widiyantoro, S., Engdahl, E.R., 1997. Evidence for deep mantle circulation from global tomography. Nature 386, 578–584.

Vidale, J.E., Benz, H.M., 1993. Seismological mapping of fine structure near the base of the Earth's mantle. Nature 361, 529–532.

Vinnik, L.P., Farra, V., Romanowicz, B., 1989. Observational evidence for diffracted SV in the shadow of the Earth's core. Geophys. Res. Lett. 16, 519–522.

Weber, M., 1993. P- and S-wave reflections from anomalies in the lowermost mantle. Geophys. J. Int. 115, 183–210.

Weber, M., Davis, J.P., 1990. Evidence of a laterally variable lower mantle structure from P- and S-waves. Geophys. J. Int. 102, 231–255.

Weber, M., Körnig, M., 1992. A search for anomalies in the lowermost mantle using seismic bulletins. Phys. Earth Planet. Int. 73, 1–28.

Wright, C., Muirhead, K.J., Dixon, A.E., 1985. The P wave velocity structure near the base of the mantle. J. Geophys. Res. 90, 623–634.

Young, C.J., Lay, T., 1987. Evidence for a shear wave velocity discontinuity in the lower mantle beneath India and the Indian Ocean. Phys. Earth Planet. Int. 49, 37–53.

Yamada, A., Nakanishi, I., 1993. The density jump across the ICB and constraints on P-reflector in the D'' layer from observation of the 1992 Chinese nuclear explosion. Geophys. Res. Lett. 20, 2195–2198.